Inverted pendulum state of a polariton Rabi oscillator

N. S. Voronova,[1,2,*] A. A. Elistratov,[3] and Yu. E. Lozovik[4,5,6]

[1]*National Research Nuclear University MEPhI (Moscow Engineering Physics Institute), 115409 Moscow, Russia*

[2]*Russian Quantum Center, 143025 Skolkovo, Moscow region, Russia*

[3]*N. L. Dukhov All-Russia Research Institute of Automatics, 127055 Moscow, Russia*

[4]*Institute for Spectroscopy RAS, 142190 Troitsk, Moscow, Russia*

[5]*Moscow Institute of Physics and Technology (State University), 141700 Dolgoprudny, Moscow region, Russia*

[6]*Moscow Institute of Electronics and Mathematics, HSE, 101000 Moscow, Russia*

(Received 2 February 2016; revised manuscript received 17 June 2016; published 11 July 2016)

Exciton-photon beats known as polariton Rabi oscillations in semiconductor microcavities are usually excited by short pulses of light. We consider a different pumping scheme, assuming a cw pumping of the Rabi oscillator from an exciton reservoir. We account for the initial pulse of light setting the phase, exciton decay due to exciton-phonon and exciton-exciton scattering, photon leakage, and blueshift of the exciton resonance due to interactions. We find nontrivial stationary solutions reminiscent of the Kapitza pendulum, where polaritons are accumulated at the upper branch while the lower branch empties.

DOI: 10.1103/PhysRevB.94.045413

I. INTRODUCTION

Light composite quasiparticles that occur due to strong coupling of quantum well excitons with photons confined in a semiconductor microcavity—exciton polaritons—have shown the ability to display macroscopic quantum coherence, including Bose-Einstein condensation [1,2], superfluidity [3–6], and varieties of bosonic Josephson phenomena [7–13]. The underlying principle of the polariton physics is that of Rabi oscillations, which are considered a signature of the strong exciton-photon coupling regime in the microcavity. From the point of view of classical optics they can be viewed as the effect of interference of two coherent electromagnetic waves emitted at different frequencies corresponding to the lower (LP) and upper (UP) polariton branches. As a result, the intensity of light emitted from the cavity oscillates with a terahertz frequency corresponding to the splitting between upper and lower polariton frequencies, which has been recently observed with high precision [14]. It is important that also the excitonic population in the system oscillates in time. The excitonic oscillations having the same frequency but opposite phase compared to photonic oscillations can be measured independently, e.g., by the pump-probe Kerr rotation technique [15].

As both excitons and cavity photons are bosons, polariton Rabi oscillations may be considered as beats in a system of two coupled harmonic oscillators. One of these oscillators is essentially nonlinear: repulsive exciton-exciton interactions result in the time-dependent blueshift of the exciton energy. This blueshift contributes to the detuning between the exciton and photon modes in microcavities.

Another important feature of the polariton system is its driven and dissipative character. Due to the finite quality factor of any realistic microcavity, cavity photons may tunnel through the Bragg mirrors—as an advantage, allowing the condensate properties to be accessed for measurement. Excitons, too, may escape from the coherent Rabi oscillator due to scattering with acoustic phonons and other excitons. In an experiment, this leakage of photons and excitons is compensated by pumping. Resonant optical pumping of the system creates photons which may be converted into excitons due to the Rabi oscillations. In addition, a nonresonant optical pumping [1] or electrical injection [16] is capable of creating an excitonic reservoir that would pump excitons into the coherent Rabi oscillator.

It has been argued recently that stimulated exciton pumping may bring the Rabi oscillator to a PT-symmetric state characterized by permanent Rabi oscillations [17]. In this work, we study the effect of exciton pumping further and demonstrate that it may lead to the appearance of a nontrivial stationary state, where the upper polariton branch is strongly occupied with exciton-polaritons while the lower polariton branch is essentially empty. This state is sustained despite the strong leakage of excitons from the upper polariton branch due to the acoustic phonon assisted scattering and exciton-exciton scattering. We draw an analogy between this peculiar solution of the nonlinear driven-dissipative Rabi problem and classical Kapitza pendulum. We discuss the critical conditions of excitation of this "inverted pendulum" state in realistic microcavities.

II. GENERAL EQUATIONS AND THE PENDULUM ANALOGY

It is convenient to describe the polariton Rabi oscillator in the exciton-photon basis (see, e.g., [18]), adopting the complex Ginzburg-Landau model of Ref. [19] for the spinless two-component system with homogeneous pumping and decay. It has been argued that a more complicated approach taking into account the dynamics of the exciton reservoir [20] can be effectively reduced when the reservoir mean-field potential is negligible and the excitation spot size is larger than the condensate size. Applicability of this model has been discussed in Refs. [21,22].

We are interested in the temporal evolution of the system, and will consider the homogeneous case when there is

*nsvoronova@mephi.ru

no external trapping potential and the pumping is spatially uniform. Assuming zero wave vector, we therefore omit all the spatial derivatives. Taking into account that the pumping of polaritons is going through their excitonic component, and the natural decay is governed by the photon leak out of the cavity, this model reads in dimensionless form as follows:

$$\begin{aligned} i\partial_t\psi_C &= \left[\epsilon_C^0 - i\kappa\right]\psi_C + \tfrac{1}{2}\,\psi_X, \\ i\partial_t\psi_X &= \left[\epsilon_X^0 + g|\psi_X|^2 + i(\gamma - \Gamma|\psi_X|^2)\right]\psi_X + \tfrac{1}{2}\,\psi_C, \end{aligned} \tag{1}$$

with $\psi_{C,X}$ the complex order parameters of cavity photons (C) and quantum well excitons (X), $\epsilon_{C,X}^0$ the bottoms of their dispersions, $g > 0$ the constant of exciton-exciton repulsive interaction. The imaginary terms in the right-hand sides read as follows: κ is the photon decay rate, and $\gamma = \gamma_X - \kappa_X$ is the effective linear gain rate of excitons, where γ_X and κ_X are the phonon-assisted exciton scattering from the reservoir and decay, respectively. $\Gamma|\psi_X|^2$ represents the exciton losses due to exciton-exciton scattering, and is usually referred to as gain saturation [19]. All energies are rescaled in the units of $\hbar\Omega_R$, lengths in the units of $\sqrt{\hbar/m_C\Omega_R}$, time in the units of Ω_R^{-1}, and the wave functions in the units of $\sqrt{\hbar/m_C\Omega_R}$ (Ω_R is the Rabi coupling strength between the photon and exciton modes, and m_C is the effective mass of cavity photon).

Using the Madelung form of the wave functions $\psi_{C,X}(t) = \sqrt{n_{C,X}(t)}\,e^{i\phi_{C,X}(t)}$ and introducing the new variables, total population $n(t) = n_C(t) + n_X(t)$, population imbalance $\rho(t) = n_C(t) - n_X(t)$, and relative phase $\phi(t) = \phi_C(t) - \phi_X(t)$, one gets the set of motion equations

$$\dot{n} = (\gamma - \kappa)n - (\gamma + \kappa)\rho - \frac{\Gamma}{2}(n-\rho)^2, \tag{2}$$

$$\dot{\rho} = -\sqrt{n^2-\rho^2}\,\sin\phi - (\gamma+\kappa)n + (\gamma-\kappa)\rho + \frac{\Gamma}{2}(n-\rho)^2, \tag{3}$$

$$\dot{\phi} = -\left(\epsilon_C^0 - \epsilon_X^0\right) + \frac{g(n-\rho)}{2} + \frac{\rho}{\sqrt{n^2-\rho^2}}\cos\phi. \tag{4}$$

The evolution equations (2)–(4) allows one to understand the effects of pumping and losses on the dynamics of the two-component condensate using the analogy of a mechanical pendulum. Its dynamics can then be visualized on a Bloch sphere of the radius n, with coordinates $x = \sqrt{n^2-\rho^2}\cos\phi$, $y = \sqrt{n^2-\rho^2}\sin\phi$, $z = \rho$, which length $\sqrt{x^2+y^2+z^2}$ is not conserved in the general case. To merge this picture with the pendulum analogy, one would have to rotate the sphere by $\pi/2$ so that the poles corresponding to the pure photonic (north) and pure excitonic (south) states are located at the new equator [see Fig. 1(a)]. Then the relative phase ϕ rotating along the old equator coincides with the tilt angle of the pendulum. Note that due to the positive sign chosen in front of the coupling terms in Eqs. (1), the gravity of the pendulum acts towards the state $\phi = \pi$ corresponding to the equilibrium condensate of lower polaritons, and the state $\phi = 0$ is at the new north pole corresponding to the upper polariton condensate. Population imbalance ρ is connected to the polar angle on the sphere as $\rho/n = \cos\theta$. This representation matches with the one used in Ref. [14].

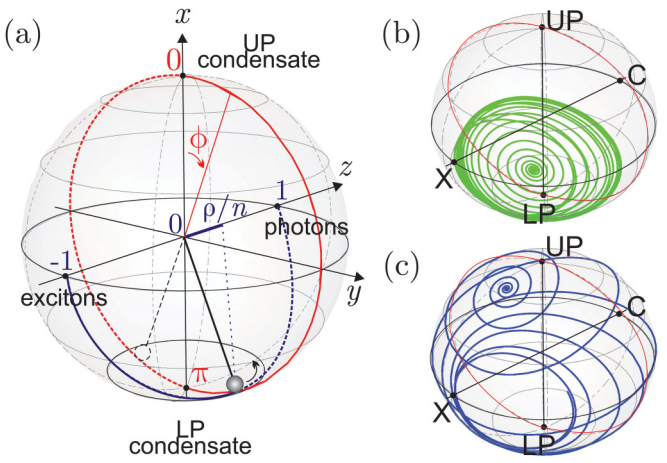

FIG. 1. (a) Bloch sphere of the radius n rotated by $\pi/2$ and the pendulum analogy for the problem. Azimuthal angle on the sphere (tilt angle of the pendulum) corresponds to the relative phase ϕ changing from 0 to 2π; polar angle θ changing from 0 to π corresponds to normalized population imbalance: $\cos\theta = \rho/n$. (b)–(c) Evolution trajectories on the normalized Bloch sphere, both starting in the point $\rho(0) = 0.5n$, $\phi(0) = \pi$ for $\kappa = 0.1$, $\gamma = 0.4 = 4\gamma^{\text{thr}}$, $g = 0.002$. (b) $\Gamma/g = 1$; the system relaxes towards the LP condensate, to the point given by (15). (c) $\Gamma/g = 0.8$; the stabilization of the "inverted pendulum" state on the UP branch. The focus point is given by (16). All energies are in units of $\hbar\Omega_R = 5$ meV.

III. ANALYSIS OF THE NONLINEAR DYNAMICS

A. Averaged evolution

In the case of no pumping and losses ($\kappa,\gamma,\Gamma \equiv 0$), Eq. (2) immediately reduces to $\dot{n} = 0$, while the equations (3), (4) acquire autonomous Hamiltonian form

$$\dot{\rho} = \frac{\partial H}{\partial\phi}, \quad \dot{\phi} = -\frac{\partial H}{\partial\rho} \tag{5}$$

with conserved energy

$$H(\phi,\rho) = \left(\epsilon_C^0 - \epsilon_X^0 - \frac{gn}{2}\right)\rho + \frac{g\rho^2}{4} + \sqrt{n^2-\rho^2}\,\cos\phi. \tag{6}$$

The condensate density n is constant, and the influence of interactions on the dynamics of bounded motion in this case is negligible [13]. For zero detuning ($\epsilon_C^0 = \epsilon_X^0$), the Hamilton equations (5) can be expressed in terms of action-angle coordinates:

$$\dot{J} = \frac{\partial H}{\partial\theta} = 0, \quad \dot{\theta} = -\frac{\partial H}{\partial J} = \omega$$

with generalized conserved momenta

$$J \equiv \frac{1}{2\pi}\oint \rho\,d\phi = \frac{2}{\pi}\int_0^{\phi^*}\sqrt{n^2 - \frac{H^2}{\cos^2\phi}}\,d\phi = n - |H|, \tag{7}$$

where $\phi^* = \arccos(H/n)$. The angular variable θ which is canonically conjugate to J is introduced as a polar angle in the phase space (ρ,ϕ), defining the position of the system on the orbit at a given moment of time. It is interesting to note that frequency ω of this Hamilton system does not depend on the amplitude, and equals ± 1. As can be seen from (7), ω changes

sign when the energy (6) crosses zero, which manifests itself in change of the rotation direction.

The pair of conjugate variables ρ and ϕ can now be defined in terms of (J,θ):

$$\rho = \mp\sqrt{J(2n-J)}\sin\theta, \tag{8}$$

$$|\cos\phi| = \frac{n-J}{\sqrt{n^2 - J(2n-J)\sin^2\theta}}. \tag{9}$$

We use the expressions (8) and (9) for approximate analytical investigation of the case when pump and dissipation are present. The transition from the variables (n,ρ,ϕ) to (n,J,θ) in the evolution equations (2)–(4) allows us to separate fast and slow motion: since the angle variable θ changes fast while the variables n and J undergo slow evolution, it is justified to average the evolution equations for $\dot{n}(t)$ and $\dot{J}(t)$ over "fast time" (assuming ergodicity of the system, we replace time averaging with averaging over θ) [23], with the result

$$\langle\dot{n}\rangle = (\gamma-\kappa)n - \frac{\Gamma}{2}n^2 - \frac{\Gamma}{4}J(2n-J), \tag{10}$$

$$\langle\dot{J}\rangle = J\left[(\gamma-\kappa) - \Gamma\left(n - \frac{J}{4}\right)\right]. \tag{11}$$

A phase portrait of the averaged evolution equations (10), (11) is presented in Fig. 2. One can see that there are two sets of trajectories which are divided by the separatrix line $J = n$, with four fixed points as follows:

$$\begin{aligned} &\text{(a)} \quad (0,0) && \text{unstable node,}\\ &\text{(b)} \quad \left(\tfrac{4}{3}\tfrac{\gamma-\kappa}{\Gamma}, \tfrac{4}{3}\tfrac{\gamma-\kappa}{\Gamma}\right) && \text{saddle,}\\ &\text{(c)} \quad \left(2\tfrac{\gamma-\kappa}{\Gamma}, 0\right) && \text{stable node,}\\ &\text{(d)} \quad \left(2\tfrac{\gamma-\kappa}{\Gamma}, 4\tfrac{\gamma-\kappa}{\Gamma}\right) && \text{stable node.} \end{aligned} \tag{12}$$

The system sets on a trajectory defined by the initial conditions $\rho(0)$ and $\phi(0)$, and gets attracted to one of the nodes, (c) or (d), which correspond to equilibrium LP and UP condensates, respectively. As follows from (8), $J = n$ corresponds to the maximal possible amplitude of population imbalance oscillations $\rho_m = n$, hence the closer the trajectory is to the separatrix, the larger is the amplitude of oscillations. It is worth noting that after the averaging, all terms containing the interaction constant g in the initial set of equations disappear. Therefore the Eqs. (10), (11) can be considered valid only for the cases when interactions are negligible. To account for interactions, one has to consider higher approximation of the Krylov-Bogoliubov averaging method [23].

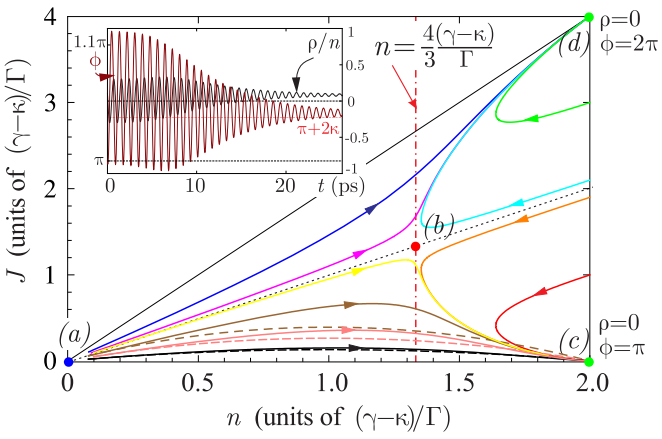

FIG. 2. Integral trajectories of the averaged set of equations (10), (11) on the phase plane (n,J) (solid lines: numerical solutions; dashed lines: analytical solutions in the small-amplitude limit). Fixed points: (a) unstable node, (b) saddle, (c) and (d) stable nodes (see the text for more details). Thin dotted line marks the separatrix $J = n$. Vertical dot-dashed line $n = 4(\gamma-\kappa)/3\Gamma$ shows the point for each trajectory when the population imbalance oscillations start to decay while the trajectories move away from the separatrix line. Inset shows numerical solutions $\rho(t)$ and $\phi(t)$ in the small-amplitude limit, for $\kappa = 0.1$, $\gamma = 0.2 = 2\gamma^{\text{thr}}$, $g = 0.002$, $\Gamma/g = 1$. All energies are given in units of $\hbar\Omega_R = 5$ meV.

B. Simulation parameters

In our modeling presented below, we assume that at the moment $t = 0$ the two-component condensate is formed by a short pulse of light exciting both LP and UP branches, setting the initial populations and phases, and will impose for all our simulations $n(0) = 1$ (which in scaled units corresponds to $\sim 10^{10}$ cm^{-2}) and $(\rho(0),\phi(0))$ on the lower semisphere of Fig. 1(a). Initial value of the action variable J can be defined from Eqs. (8) and (9), and it reads $J(0) = n(0) - \sqrt{n^2(0) - \rho^2(0)}\cos S(0)$. Note that for the sake of simplicity, we consider only the case of zero energy detuning $\epsilon_C^0 - \epsilon_X^0 = 0$.

Before describing the different regimes of the dynamics, it is convenient to approximately define the parameters' values. We take the interaction constant $g = 0.002$ (in scaled units, 0.015 meV μm^2). Values of the decay rate κ in our simulations vary from 0.02 to 0.1 (which corresponds to 0.1 to 0.5 meV). This is consistent with the experiments to date reporting the cavity photon linewidth at low excitation powers; see, e.g., Ref. [1]. The linear gain rate for excitons at threshold is equal to $\gamma^{\text{thr}} = \kappa$, so we use the values from just above threshold up to 20 times the threshold pump power, $1 < \gamma/\gamma^{\text{thr}} < 20$. Obviously, if $\gamma < \kappa$, the condensate density will decay to zero. At last, the value of the saturation coefficient Γ, which is most important as it brings the imaginary nonlinearity to the system, is unclear. If Γ is too small, the condensate population n grows (given $\gamma > \kappa$) until reaching the equilibrium value $n_\infty = \gamma/\Gamma$ and the population imbalance ρ shifts to $-n$ as all photons leak out of the cavity and the system becomes filled with excitons. If Γ is very high (larger than the interaction constant g), i.e., the saturation is fast, the total population tends to the equilibrium value $n_\infty = 2(\gamma-\kappa)/\Gamma$ while the (normalized) population imbalance performs small-amplitude, fast-decaying oscillations around $gn_\infty/2$. At further increase of Γ, the dynamics does not change except for speeding-up of the oscillations' decay. As we indeed see in our simulations, the ratio Γ/g is one of the values determining the type of dynamics.

It has been argued [24,25] that the imaginary nonlinearity $\Gamma|\psi_X|^2$ in Eq. (1) should be 3 to 40 times smaller than the real nonlinearity $g|\psi_X|^2$. For the present discussion, we will use the values in the range $0.025 < \Gamma/g < 1$.

C. Small-amplitude oscillations

In the case when amplitude of oscillations is small during the whole evolution time (which corresponds to integral trajectories far from the separatrix in Fig. 2), the set of equations (2)–(4) allows analytical solution. Imposing $\rho \ll n$ in (2) or, equivalently, $J \ll n$ in (10), one gets

$$n(t) = \frac{\gamma-\kappa}{\Gamma}\left[1+\tanh\left\{\frac{\gamma-\kappa}{2}(t+t_0)\right\}\right], \qquad (13)$$

where $t_0 = 2\,\mathrm{arctanh}[\Gamma n(0)/(\gamma-\kappa)-1]/(\gamma-\kappa)$. At $t \to \infty$, this solution gives the limiting value for the condensate population, $n_\infty = 2(\gamma-\kappa)/\Gamma$. Similarly, assuming $J \ll n$ in (11), one gets

$$J(t) = J(0)\,\frac{\cosh^2[(\gamma-\kappa)t_0/2]}{\cosh^2[(\gamma-\kappa)(t+t_0)/2]}. \qquad (14)$$

The analytical solutions for trajectories corresponding to the small-amplitude limit are plotted in Fig. 2 as dashed lines. Numerical solutions for $\rho(t)$ and $\phi(t)$ in the small-amplitude limit are shown in the inset of Fig. 2. A typical trajectory of the pendulum on the Bloch sphere for this case is plotted in Fig. 1(b) for $\gamma = 4\gamma^{\mathrm{thr}}$ and $\Gamma/g = 1$. As explained below, the trajectories starting from the basin of attraction of the lower fixed point (which exists at large values of Γ/g) flow towards the unstable limit cycle, and then relax towards the stable lower focus which is located on the "photon" semisphere ($\rho > 0$, $\phi > \pi$).

D. Fixed point coordinates and stability

Using the stable node coordinates $\rho = 0$, $\phi = \pi$ (see Fig. 2) as a starting point of unaveraged evolution analysis, we linearize Eqs. (3) and (4) in the region $\rho/n \ll 1$ and $|\phi-\pi| \ll 1$. In the adiabatic approximation, assuming $n(t)$ a known, slowly changing function given by (13), we get damped-driven pendulum equations for $\rho(t)$ and $\phi(t)$. From those equations we extract the damping rates of population imbalance $\beta_\rho = 3(\Gamma n)/4 - (\gamma-\kappa)$ and relative phase $\beta_\phi = (\gamma-\kappa-\Gamma n/2)/(2+gn)$ and the new approximate coordinates of the lower focus:

$$\left(\frac{\rho}{n}\right)_\infty^{\mathrm{LP}} \simeq \frac{1}{1+\frac{\Gamma}{g(\gamma-\kappa)}}, \quad \phi_\infty^{\mathrm{LP}} \simeq \pi + 2\kappa. \qquad (15)$$

It is worth noting that the damping of the oscillations is density-dependent, which brings the analogy with the van der Pol oscillator: as long as $n < 4(\gamma-\kappa)/3\Gamma$, the oscillations of population imbalance are amplified, and they start to decay only after n passes the saddle point shown in Fig. 2. Oscillations of the relative phase are damped for all $n < n_\infty = 2(\gamma-\kappa)/\Gamma$. Similarly linearizing the evolution equations around the upper fixed point of the averaged dynamics, $\rho = 0$, $\phi = 2\pi k$ ($k \in \mathbb{Z}$), for the upper focus one has

$$\left(\frac{\rho}{n}\right)_\infty^{\mathrm{UP}} \simeq -\frac{1}{1+\frac{\Gamma}{g(\gamma-\kappa)}}, \quad \phi_\infty^{\mathrm{UP}} \simeq 2\pi k - 2\kappa. \qquad (16)$$

As follows from these results, the regime of small-amplitude damped oscillations can take place only if $2\kappa \ll 1$ and $g(\gamma-\kappa)/\Gamma \ll 1$, i.e., at low decay rate, low pump powers, and relatively large saturation coefficients (comparable to g). Given κ is small, if Γ/g is decreased at a fixed value of γ or, alternatively, the gain rate γ is increased at fixed Γ/g, the initial assumption $\rho/n \ll 1$ becomes invalid. Note, however, that for the case of no interactions ($g = 0$), for arbitrary values of the parameters one has $n \to 2(\gamma-\kappa)/\Gamma$, $\langle\rho\rangle = 0$, and $\langle S\rangle = \pi + 2\kappa$, even for large $\rho(0)$ comparable to $n(0)$ (then the initial amplitude of oscillations is not small).

To obtain information about the stability of the fixed points, we graphically determine the exact foci coordinates n_∞, ρ_∞, and ϕ_∞ by imposing $\dot n = 0$, $\dot\rho = 0$, and $\dot\phi = 0$ for a steady state at $t \to \infty$ in the evolution equations (2)–(4). Each possible evolution line ends at a point on the resulting surface $\rho(n)$ in the 3D space (n,ρ,ϕ):

$$(\gamma-\kappa)n - (\gamma+\kappa)\rho - \frac{\Gamma}{2}(n-\rho)^2 = 0. \qquad (17)$$

Intersection of this surface with the lines

$$\pm\sqrt{n^2-\rho^2}\sqrt{1-\frac{g^2}{4}\frac{(n-\rho)^2(n^2-\rho^2)}{\rho^2}} + (\gamma+\kappa)n - (\gamma-\kappa)\rho + \frac{\Gamma}{2}(n-\rho)^2 = 0 \qquad (18)$$

gives the coordinates (n,ρ,ϕ) of the two equilibria of the dynamical system. Linearizing the system in the vicinity of the fixed points, one gets a cubic equation for the three eigenvalues of the Jacobian matrix, which has one real root $\lambda_1 < 0$ and two complex conjugate roots $\lambda_{2,3}$. If $\lambda_1 < 0$ and $\mathrm{Re}(\lambda_{2,3}) < 0$, then the focus in 3D space is stable (attracting the trajectories), and if $\mathrm{Re}(\lambda_{2,3}) > 0$, the focus is unstable (repulsing the trajectories). Changing the parameters and defining the coordinates $(n_\infty, \rho_\infty, \phi_\infty)$ of the fixed points, we look for the values of γ, κ, and Γ, at which the complex eigenvalues cross the imaginary axis [i.e., $\mathrm{Re}(\lambda_{2,3}) = 0$]. For all values of the parameters that we consider, we find that the upper focus given approximately by (16) is always stable, while for the lower focus (15) each pair (κ,γ) reveals values of Γ at which the equilibrium LP condensate state becomes unstable.

E. Inverted pendulum state

If gain rate $\gamma/\gamma^{\mathrm{thr}}$ is increased at fixed Γ/g, or, equivalently, the saturation parameter Γ decreased at fixed γ, the condensate population will grow and hence the interparticle interactions strongly alter the dynamics.

As mentioned above, as long as density is small, damping β_ρ is negative, and it reaches zero when $n(t)$ passes the saddle point on the averaged diagram (see Fig. 2). For unaveraged trajectories in 3D phase space (n,ρ,ϕ) this point corresponds to a *saddle limit cycle*. When trajectories approach this limit cycle, $\langle n\rangle$ stays approximately constant, while on the phase

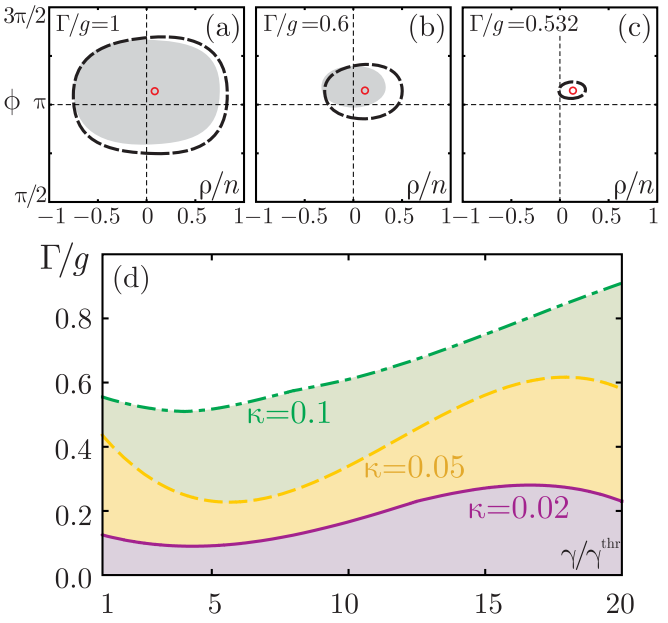

FIG. 3. (a)–(c) Basin of attraction of the lower fixed point (red circle) and projection of the saddle limit cycle (black dashed line) for Γ/g as indicated on the panels and other parameters the same as in Fig. 2. Initial values of (ρ,ϕ) that get attracted to the fixed point (15) are colored gray; others which flow towards the limit cycle and get attracted to the upper fixed point [see Fig. 4(c)] are white. (d) Bifurcation diagram showing the regions of stability of the lower fixed point and existence of the trajectories flowing towards the LP condensate, for three values of decay rate κ as marked. Regions above the lines correspond to the existence of points flowing towards the LP condensate. For colored regions below the lines, any starting point gets attracted to the upper focus.

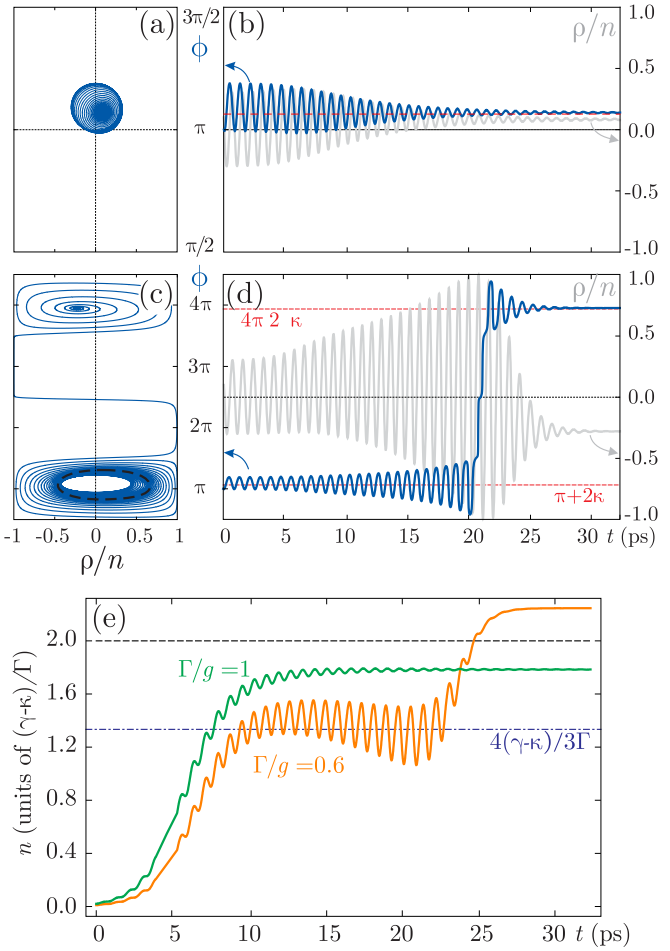

FIG. 4. Numerical solutions of the evolution equations (2)–(4) for $\kappa = 0.1$, $\gamma = 0.2 = 2\gamma^{\rm thr}$, and initial values $\rho(0) = 0.35n$, $\phi(0) = \pi + 2\kappa$. (a) Trajectory projection on the phase plane $(\rho/n,\phi)$ for $\Gamma/g = 1$, and (b) corresponding evolutions $\rho(t)$ (gray) and $\phi(t)$ (blue). The red dashed line indicates the focus coordinate $\phi_\infty^{\rm LP}$ given approximately by (15). (c) Phase-plane portrait projection for $\Gamma/g = 0.6$ showing crowding of the trajectories in the area of the limit cycle projection (black dashed line) and consequent stabilization of the inverted pendulum state at $\phi \simeq 4\pi - 2\kappa$. (d) Corresponding evolutions $\rho(t)$ (gray) and $\phi(t)$ (blue). The red dashed lines show $\phi_\infty^{\rm LP}$ and $\phi_\infty^{\rm UP}$ given by (15) and (16), respectively. (e) Total density n against time for $\Gamma/g = 1$ and 0.6 as marked. When passing the saddle limit cycle, $n(t)$ oscillates with $\langle n\rangle \approx 4(\gamma-\kappa)/3\Gamma$ [see the saddle point (c) in Fig. 2]. Other parameters the same as used in Figs. 1 and 2.

plane (ρ,ϕ) the system is orbiting the same line without damping, then gets repulsed from it to get finally attracted to one of the stable equilibria. The projection of the limit cycle on the plane (ρ,ϕ) and basin of attraction of the lower fixed point are shown in Figs. 3(a)–3(c). As one can see, for large values of Γ (in the units of g), there can be two regimes of the dynamics depending on the starting point of the phase plane (ρ,ϕ): if the trajectory starts from the basin of attraction, the dynamics is that of relaxation oscillations shown in the inset of Fig. 2 and Figs. 4(a) and 4(b); the system then relaxes towards the equilibrium LP condensate ($\phi \simeq \pi$). Contrary to this, if the system is prepared in the initial state lying outside the basin of attraction, the trajectory will flow towards the limit cycle, and then through the series of large-amplitude oscillations wind up towards the upper focus [see the simulation results in Figs. 4(c) and 4(d)], which corresponds to the upper polariton condensate ($\phi \simeq 2\pi k$, $k \in \mathbb{Z}$). With the decrease of Γ, the basin of attraction shrinks, and at some critical value of Γ, the LP state becomes unstable, the limit cycle disappears, and all trajectories get attracted to the UP state. The limit cycle exists as long as there are points being attracted to the lower equilibrium, and disappears in the moment when it loses stability. For trajectory projections on the 2D phase plane (ρ,ϕ), one then has a subcritical Hopf bifurcation in which a small-amplitude limit cycle is branching from a fixed point which changes the type of stability (for more details see, e.g., Ref. [26]). The bifurcation diagram plotted in Fig. 3(d) shows the parameters at which the system stabilizes in the UP state regardless of the initial conditions.

In the pendulum analogy, the transition to the upper equilibrium can be compared with the Kapitza pendulum which stabilizes in the state upwards while gravity is acting downwards [27]. The corresponding evolution on the sphere (the trajectory of the pendulum) is presented in Fig. 1(c). However, for the Kapitza pendulum, the inverted state stabilizes due to fast vibrations of the suspension point, while in our case the oscillations are that of the pendulum length (the radius of the Bloch sphere).

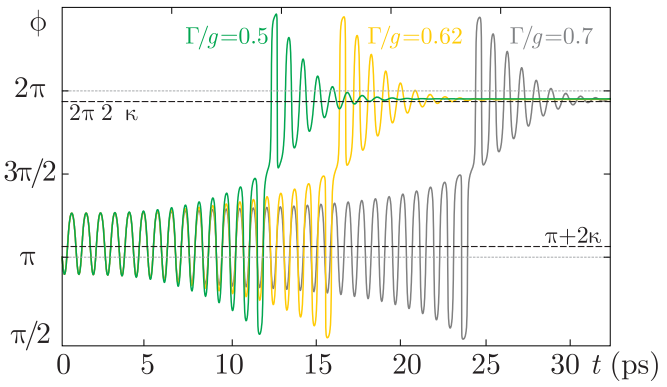

FIG. 5. Relative phase ϕ against time for three values of Γ/g as marked, for $\rho(0) = 0.5n$, $\phi(0) = \pi$. Other parameters are the same as in Figs. 1 and 2.

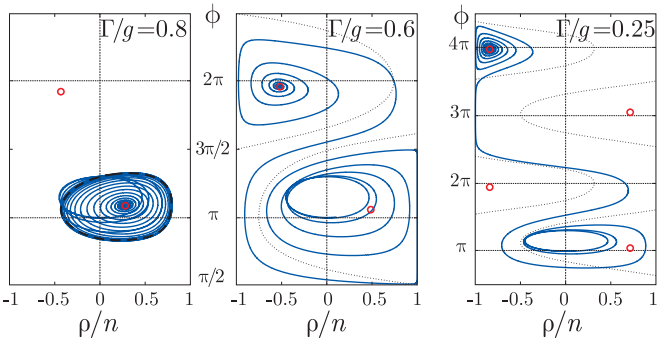

FIG. 6. Phase-plane portraits [projections of 3D trajectories on the plane $(\rho/n,\phi)$] for $\kappa = 0.1$, $\gamma = 0.4 = 4\gamma^{\rm thr}$, and Γ/g as indicated on the panels. Initial conditions: $\rho(0) = 0.1n$, $\phi(0) = \pi$. Other parameters are the same as used in Figs. 1 and 2. The black dashed line marks the projection of the saddle limit cycle where it exists; the red circles indicate the fixed points. When the starting point belongs to the basin of attraction of the lower equilibrium, after reaching the limit cycle the trajectory winds up to the stable LP state (see leftmost panel). Otherwise the system arrives at the "inverted pendulum" (UP) state. Thin dotted lines in the central and rightmost panels schematically mark the corridor of infinite motion (see the text for more details).

The case of relaxation oscillations discussed in the Sec. III C is shown in Fig. 4 in comparison with the "inverted pendulum" scenario. We fix the initial conditions $\rho(0) = 0.35n$, $\phi(0) = \pi + 2\kappa$, and pumping $\gamma = 2\gamma^{\rm thr}$, and change the nonlinear loss rate Γ. While for the both cases the starting point lies inside the limit cycle projection on the phase portrait (ρ,ϕ), for $\Gamma/g = 1$ [see Figs. 4(a) and 4(b)] it belongs to the basin of attraction of the lower focus, in contrast to the case of $\Gamma/g = 0.6$ shown in Figs. 4(c) and 4(d) where the population imbalance oscillations amplify up to their maximum amplitude $\rho_m = n$. Note that when the amplitude is large, the analytical damping rates found in the Sec. III D are no longer correct, and the oscillations of the relative phase start to amplify as well. When $n(t)$ reaches its saddle point, it starts to oscillate around $\langle n\rangle \approx 4(\gamma - \kappa)/3\Gamma$ [see Fig. 4(e)], while the trajectories on the phase plane (ρ,ϕ) get crowded around the saddle limit cycle projection shown as the black dashed line in Fig. 4(c). After leaving the limit cycle, the evolution line relaxes fast towards the upper stable focus (16). The times at which this stabilization occurs also depend on the ratio Γ/g (see Fig. 5).

In Fig. 6, we increase the pumping $\gamma = 4\gamma^{\rm thr}$, and investigate again the system behavior for different values of the ratio Γ/g at fixed initial conditions $\rho(0) = 0.1n$, $\phi(0) = \pi$. Qualitatively, the dynamical regimes are the same as for small γ, although the dynamics is much faster, and the UP state is much more shifted towards the exciton state, in agreement with (16). However, in Fig. 6 we notice that with the decrease of Γ and destabilization of the LP equilibrium, the transition to the UP state happens without population imbalance amplitude reaching its maximum possible value n. The smaller is Γ compared to g, the smaller is the amplitude of oscillations at which the transition to the upper focus happens. One could understand this effect as follows. With higher pumping, the population of the condensate increases, and the blueshift value $g|\psi_X|^2$ adds more to the (negative) detuning between the photon and exciton modes. As we have shown in our previous work [13] for a conservative system without gain and dissipation, when the detuning increases, there can be two regimes of internal oscillations: that of Rabi oscillations with the relative phase oscillating around π (and trajectories on the phase plane orbiting the fixed points), and the regime of unbound motion characterized by the running relative phase, when the trajectory on the phase plane becomes reminiscent of the ones shown in the central and rightmost panels of Fig. 6, however infinite (not decaying towards the foci). Here, one could say that the transition from oscillations around the lower focus to oscillations around the upper focus happens via the running phase regime. When the density increases (due to the pump increase or the losses decrease), the effective detuning grows, and the area of bounded motion (closed orbits) on the phase plane (ρ,ϕ) reduces, while the corridor of infinite motion (shown as thin dotted lines in Fig. 6) widens. Hence the smaller amplitude of ρ is needed to get into this area and consequently transit towards one of the attracting foci $\phi_\infty = 2\pi k - 2\kappa$ $(k \in \mathbb{Z})$. The foci given by $\phi_\infty = \pi(2k+1) + 2\kappa$ $(k \in \mathbb{Z})$ are repulsive, as one can see in the rightmost panel of Fig. 6. For more details and discussion of the regime of the running relative phase please see Refs. [13,28].

IV. CONCLUDING REMARKS

In this work, we have demonstrated theoretically the existence of an "unstable van der Pol" limit cycle and an inverted stationary state of a polariton Rabi oscillator driven by the cw pumping via the excitonic reservoir. The formation of such an "inverted pendulum" state can be intuitively understood as follows. In the C-X basis, we include the pumping of the system from the reservoir in the equation for ψ_X, which corresponds to feeding of the excitonic fraction of polaritons. Since the UP state is more "exciton-like" (has an increased exciton fraction compared to LP) due to the blueshift, this kind of pumping favors the upper state, while the "photon-like" LP state is getting depleted due to leakage of photons from the cavity. This process is limited and stabilized by the nonlinear exciton dissipation process. The dynamics is then determined by the competition of real and imaginary

nonlinearities in Eq. (1). When nonlinear exciton losses $\Gamma|\psi_X|^2$ are large enough compared to the blueshift $g|\psi_X|^2$, the system relaxes towards the LP condensate. If Γ is low, however, the excitonic fraction of the polariton gas grows, which leads to the accumulation of particles on the UP branch. The described effects are essentially nonlinear: the stationary populations of the UP and LP states are dependent on the dynamical balance between exciton pumping and exciton-exciton scattering. It is worth mentioning that the Kapitza pendulum-like effects were also shown for atomic condensates in oscillating double-well potentials [29]; however here they have a completely different nature.

The problem considered here is strictly homogeneous. When taking into account the spatial degree of freedom, internal oscillations create density waves in space, similar to the ones modeled numerically in Ref. [30]. The dispersion law for these waves at sufficiently small momenta is expected to coincide with the dispersion curve of the upper polaritons. Correspondingly, for long-wavelength waves, locally, the phenomena predicted in this paper should take place. Investigation of short-wavelength waves of such type or the influence of inhomogeneities caused by small pump spot size or disorder is subject to a future study.

It has been argued recently that microcavity polaritons present a solid-state quantum simulator platform [31]. Quantum simulators can provide insights into complex physical problems by mimicking their nature in a controlled setting. Exciton polaritons enable one to define almost arbitrary lattice structures in 2 and 1 dimensions, and in this open and dissipative system excited state condensation can be readily obtained [31–33]. In this work, we show that condensation in an excited UP state is possible in a homogeneous two-dimensional system, thanks to a specific pumping scheme and the peculiar physics of polaritons, stemming from their part-light part-matter nature. Our results therefore are widely relevant for the interdisciplinary field of quantum simulations.

ACKNOWLEDGMENTS

We would like to thank Alexey Kavokin and Sven Höfling for discussions. The work of N.S.V. is financially supported by the Russian Foundation for Basic Research, according to the research Project No. 16-32-60066 mol_a_dk, and the Competitiveness Program of NRNU MEPhI. Yu.E.L. is supported by the Program of Basic Research of the High School of Economy.

[1] J. Kasprzak, M. Richard, S. Kundemann, A. Baas, P. Jeambrun, J. M. J. Keeling, F. M. Marchetti, M. H. Szymanska, R. Andre, J. L. Staehli, V. Savona, P. B. Littlewood, B. Deveaud, and Le Si Dang, Nature (London) **443**, 409 (2006).

[2] R. Balili, V. Hartwell, D. Snoke, L. Pfeiffer, and K. West, Science **316**, 1007 (2007).

[3] I. Carusotto and C. Ciuti, Phys. Rev. Lett. **93**, 166401 (2004).

[4] A. Amo, D. Sanvitto, F. P. Laussy, D. Ballarini, E. del Valle, M. D. Martin, A. Lemaître, J. Bloch, D. N. Krizhanovskii, M. S. Skolnick, C. Tejedor, and L. Viña, Nature (London) **457**, 291 (2009).

[5] A. Amo, J. Lefrère, S. Pigeon, C. Adrados, C. Ciuti, I. Carusotto, R. Houdré, E. Giacobino, and A. Bramati, Nat. Phys. **5**, 805 (2009).

[6] A. Amo, S. Pigeon, D. Sanvitto, V. G. Sala, R. Hivet, I. Carusotto, F. Pisanello, G. Leménager, R. Houdré, E. Giacobino, C. Ciuti, and A. Bramati, Science **332**, 1167 (2011).

[7] M. Wouters, Phys. Rev. B **77**, 121302(R) (2008).

[8] D. Sarchi, I. Carusotto, M. Wouters, and V. Savona, Phys. Rev. B **77**, 125324 (2008).

[9] I. A. Shelykh, D. D. Solnyshkov, G. Pavlovic, and G. Malpuech, Phys. Rev. B **78**, 041302(R) (2008).

[10] D. Read, Y. G. Rubo, and A. V. Kavokin, Phys. Rev. B **81**, 235315 (2010).

[11] K. G. Lagoudakis, B. Pietka, M. Wouters, R. André, and B. Deveaud-Plédran, Phys. Rev. Lett. **105**, 120403 (2010).

[12] M. Abbarchi, A. Amo, V. G. Sala, D. D. Solnyshkov, H. Flayac, L. Ferrier, I. Sagnes, E. Galopin, A. Lemaître, G. Malpuech, and L. Bloch, Nat. Phys. **9**, 275 (2013).

[13] N. S. Voronova, A. A. Elistratov, and Yu. E. Lozovik, Phys. Rev. Lett. **115**, 186402 (2015).

[14] L. Dominici, D. Colas, S. Donati, J. P. Restrepo Cuartas, M. De Giorgi, D. Ballarini, G. Guirales, J. C. Lopez Carreno, A. Bramati, G. Gigli, E. del Valle, F. P. Laussy, and D. Sanvitto, Phys. Rev. Lett. **113**, 226401 (2014).

[15] A. Brunetti, M. Vladimirova, D. Scalbert, M. Nawrocki, A. V. Kavokin, I. A. Shelykh, and J. Bloch, Phys. Rev. B **74**, 241101(R) (2006).

[16] C. Schneider, A. Rahimi-Iman, N. Y. Kim, J. Fischer, I. G. Savenko, M. Amthor, M. Lermer, A. Wolf, L. Worschech, V. D. Kulakovskii, I. A. Shelykh, M. Kamp, S. Reitzenstein, A. Forchel, Y. Yamamoto, and S. Höfling, Nature (London) **497**, 348 (2013).

[17] I. Y. Chestnov, S. S. Demirchyan, S. M. Arakelian, A. P. Alodjants, Y. G. Rubo, and A. V. Kavokin, Sci. Rep. **6**, 19551 (2016).

[18] C. Ciuti and I. Carusotto, Phys. Status Solidi B **242**, 2224 (2005).

[19] M. O. Borgh, J. Keeling, and N. G. Berloff, Phys. Rev. B **81**, 235302 (2010).

[20] M. Wouters and I. Carusotto, Phys. Rev. Lett. **99**, 140402 (2007).

[21] H. Haug, T. D. Doan, and D. B. Tran Thoai, Phys. Rev. B **89**, 155302 (2014).

[22] D. D. Solnyshkov, H. Terças, K. Dini, and G. Malpuech, Phys. Rev. A **89**, 033626 (2014).

[23] N. Bogoliubov, *Asymptotic Methods in the Theory of Non-Linear Oscillations* (Gordon and Breach, Paris, 1961).

[24] J. Keeling and N. G. Berloff, Phys. Rev. Lett. **100**, 250401 (2008).

[25] P. R. Eastham, Phys. Rev. B **78**, 035319 (2008).

[26] R. Sagdeev, D. Usikov, and G. Zaslavsky, *Nonlinear Physics: From Pendulum to Turbulence and Chaos* (Harwood Academic Publishers, Chur, Switzerland, 1988).

[27] *Collected Papers of P. L. Kapitza*, edited by D. ter Haar, Vol. 2 (Pergamon, Oxford, 1965).

[28] A. Rahmani and F. P. Laussy, arXiv:1603.05971.

[29] E. Boukobza, M. G. Moore, D. Cohen, and A. Vardi, Phys. Rev. Lett. **104**, 240402 (2010).
[30] T. C. H. Liew, Y. G. Rubo, and A. V. Kavokin, Phys. Rev. B **90**, 245309 (2014).
[31] N. Y. Kim and Y. Yamamoto, arXiv:1510.08203.
[32] N. Y. Kim, K. Kusudo, C. Wu, N. Masumoto, A. Löffler, S. Höfling, N. Kumada, L. Worschech, A. Forchel, and Y. Yamamoto, Nat. Phys. **7**, 681 (2011).
[33] C. Schneider, K. Winkler, M. D. Fraser, M. Kamp, Y. Yamamoto, E. A. Ostrovskaya, and S. Höfling, arXiv:1510.07540.